Hindawi
Mathematical Problems in Engineering
Volume 2019, Article ID 9158093, 14 pages
https://doi.org/10.1155/2019/9158093

Research Article

Entropy Generation in MHD Radiative Flow of CNTs Casson Nanofluid in Rotating Channels with Heat Source/Sink

Poom Kumam[1,2,3] **Zahir Shah**[4] **Abdullah Dawar**[5] **Haroon Ur Rasheed**[6] **and Saeed Islam**[2]

[1]*KMUTTFixed Point Research Laboratory, Room SCL 802 Fixed Point Laboratory, Science Laboratory Building, Department of Mathematics, Faculty of Science, King Mongkut's University of Technology Thonburi (KMUTT), 126 Pracha-Uthit Road, Bang Mod, Thrung Khru, Bangkok 10140, Thailand*
[2]*KMUTT-Fixed Point Theory and Applications Research Group, Theoretical and Computational Science Center (TaCS), Science Laboratory Building, Faculty of Science, King Mongkut's University of Technology Thonburi (KMUTT), 126 Pracha-Uthit Road, Bang Mod, Thrung Khru, Bangkok 10140, Thailand*
[3]*Department of Medical Research, China Medical University Hospital, China Medical University, Taichung 40402, Taiwan*
[4]*Department of Mathematics, Abdul Wali Khan University, Mardan 23200, KP, Pakistan*
[5]*Department of Mathematics, Qurtuba University of Science and Information Technology, Peshawar 25000, KP, Pakistan*
[6]*Sarhad University of Sciences and Information Technology, Peshawar, Pakistan*

Correspondence should be addressed to Poom Kumam; poom.kum@kmutt.ac.th and Haroon Ur Rasheed; haroon.csit@suit.edu.pk

Received 6 October 2018; Revised 28 November 2018; Accepted 31 January 2019; Published 26 March 2019

Academic Editor: Chaudry M. Khalique

Copyright © 2019 Poom Kumam et al. This is an open access article distributed under the Creative Commons Attribution License, which permits unrestricted use, distribution, and reproduction in any medium, provided the original work is properly cited.

We presented the applications of entropy generation for SWCNTs and MWCNTs based on kerosene oil for Casson nanofluid flow by rotating channels. Kerosene oil has advanced thermal conductivity and exclusive features and has a lot of practical uses due to its unique behavior. That is why we have used kerosene oil as a based fluid. For the entropy generation second law of thermodynamics is applied and implemented for the nanofluid transport mechanism. In the presence of magnetic field, the effects of thermal radiations and heat source/sink on the temperature profiles are studied. The fluid flow is supposed in steady state. With the help of suitable similitude parameters, the leading equations have been transformed to a set of differential equations. The solution of the modeled problem has been carried out with the homotopic approach. The physical properties of carbon nanotubes are shown through tables. The effects of the imbedded physical parameters on the velocities, temperature, entropy generation rate, and Bejan number profiles are investigated and presented through graphs. Moreover, the impact of significant parameters on surface drag force and heat transfer rate is tabulated.

1. Introduction

Nanofluid is the potential heat transfer fluid which is one of the fundamental fragments of nanotechnology. Engine transmission oil, boiler exhaust flue gas recovery, cooling of electronics, nuclear systems cooling, nanofluids in drilling, defense, high-power lasers, space, biomedical applications, microwave tubes, drilling, thermal storage, lubrications, drag reductions, solar water heating, in diesel electric generator as jacket water coolant, heating and cooling of buildings, engine cooling, nanofluids in transformer cooling oil, cooling of welding, refrigeration (chillers, domestic refrigerator), etc. are the applications of carbon nanotubes (CNTs). These applications got the researchers attention to work on CNTs. Choi [1] has presented the idea of nanofluids for the first time by dipping the nanometer sized particle into the base fluid. The single-walled carbon nanotubes (SWCNTs) have higher heat transfer rate and surface drag force than multiwalled carbon nanotubes (MWCNTs) reported by Haq et al. [2]. Liu et al. [3] studied the synthetic engine oil and ethylene glycol in the presence of MWCNTs. They claimed that ethylene glycol with CNTs has higher thermal conductivity. Nadeem and Lee [4] presented the concept of nanofluid past over an exponentially stretching sheet. The boundary layer

flow of nanoparticles over a stretching/shrinking surface is studied by Nadeem and Lee [5–8]. The mathematical model for the examination of nanofluids flow was established by Boungiorno [9]. Sheikholeslami [10–15] experimentally and theoretically studied the properties, applications, and impacts of nanofluids. Using mesoscopic approach, Sheikholeslami and Rokni [16–19] examined simulation of nanofluids and CuOeH2O nanofluid in a curved porous enclosure. Elias et al. [20] have inspected the impact of shape on heat transmission.

As the time passes the geometry of the problem translated to more complex nature. One factor of the complexity of the problem geometry is the magnetic effect. Fluids coming under this umbrella are called magneto fluids, for example, liquid metals, plasmas, salt water, and electrolytes. Crystal growth, cooling of devices, magnetic drug targeting, and electromagnetic casting are the real-world uses of magnetic hydrodynamics (MHD) in the field of engineering and technology. Magnetic hydrodynamics (MHD) was proposed by Hannes Alfven [21]. Hayat et al. [22] studied the Magneto hydrodynamic flow of Casson nanofluid effects past over a stretched surface. Ali et al. [23] examined the blood flow of Casson fluid under the impact of Magneto hydrodynamics (MHD) in axisymmetric cylindrical tube. Shah et al. [24–26] examined the MHD nanofluid in rotating systems. Dawar et al. [27] examined the MHD carbon nanotube Casson nanofluid and radiative heat transfer in rotating channels. Kumar et al. [28] examined the MHD Williamson fluid over a curved sheet under the impact of nonthermal heat source/sink. Kumaran and Sandeep [29] studied the parabolic flow of MHD Casson and Williamson fluids under the impact of thermophoresis and Brownian motion parameters. The impact of Brownian motion and thermophoresis on bioconvective flow of nanoliquids has been examined by Kumar et al. [30]. The other related studies of Kumar et al. can be seen in [31–36].

Casson fluid model characterizes a shear retreating fluid which is presumed to obligate infinite viscosity at zero rate of shear stress. This famous model after the initiation becomes the main point of interest for researchers. Development has been made in model by adding extra agents to the geometry of the modeled problem. Recently, Mehmood et al. [37, 38] numerically inspected Casson micropolar fluid over a stretched sheet with internal heat transmission. Singh Megahe et al. [39] examined the film flow of Casson fluid in the existence of varied heat flux using slip velocity. Abolbashari et al. [40] have studied the Casson nanofluid with entropy generation. The study about the fundamental models of CNTs can be read in [41–45].

The goal of this research work is to examine the nanoparticles of SWCNTs and MWCNTs Casson fluid between two rotating parallel plate. The kerosene oil is taken as base fluid. The solution of the modeled problem has been carried out with the homotopic approach. Homotopy analysis method (HAM) is used due to better results. Many researchers [46–55] used HAM. The influence of thermal radiations, magnetic parameter, and heat source/sink is taken into account. The effect of all embedded parameters on velocities and temperature profiles has been studied graphically and discussed in detail.

2. Some Basic Thermal Conductivities and Fluid Models

Model of thermal conductivity for CNTs proposed by Maxwell [41] defined as

$$\frac{k_{nf}}{k_f} = 1 + \frac{3\left(\left(k_{nf}-k_f\right)/k_f\right)\varphi}{\left(\left(k_{nf}-k_f\right)/k_f+2\right)-\left(\left(k_{nf}-k_f\right)/k_f-1\right)\varphi}. \tag{1}$$

where φ is known as nanoparticle volume fraction.

Model of thermal conductivity for CNTs proposed by Jeffery [42] is the form:

$$\frac{k_{nf}}{k_f} = 1 + 3\left(\frac{k_{nf}-k_f}{k_{nf}+2k_f}\right)\varphi + \left(3\left(\frac{k_{nf}-k_f}{k_{nf}+2k_f}\right)^2 + \frac{3}{4}\left(\frac{k_{nf}-k_f}{k_{nf}+2k_f}\right)^3 + \cdots\right)\varphi^2. \tag{2}$$

Davis [43] modified Jeffery's model as

$$\frac{k_{nf}}{k_f} = 1 + \frac{3\left(\left(k_{nf}-k_f\right)/k_f\right)\varphi}{\left(\left(k_{nf}+2k_f\right)/k_f\right)-\left(\left(k_{nf}-k_f\right)/k_f\right)\varphi}\left\{\varphi + \varphi\left(\frac{k_{nf}-k_f}{k_f}\right)\varphi^2 + \frac{k_{nf}-k_f}{k_f}\left(\varphi^3\right)\right\}. \tag{3}$$

Hamilton and Crosser [44] proposed a new model defined as

$$\frac{k_{nf}}{k_f} = \frac{k_{nf}/k_f + (\Phi-1) - \left(\left(k_{nf}-1\right)/k_f\right)(\Phi-1)\varphi}{k_{nf}/k_f + (\Phi-1) - \left(\left(k_{nf}-1\right)/k_f\right)\varphi}. \tag{4}$$

Models (1)-(3) did not depend on shape of particles and deliver the approximations of thermal conductivity for small φ. On the other hand, model (4) depends on the shape of particles. The symbol Φ in (4) represents shape factor of the particles. Recently, Xue [45] proposed a model of a very large axial ratio recompensing the CNTs space distribution.

$$\frac{k_{nf}}{k_f} = \frac{1-\varphi+2\left(\left(k_{nf}/\left(k_{nf}-k_f\right)\right)\ln\left(\left(k_{nf}+k_f\right)/2k_f\right)\right)\varphi}{1-\varphi+2\left(\left(k_f/\left(k_{nf}-k_f\right)\right)\ln\left(\left(k_{nf}+k_f\right)/2k_f\right)\right)\varphi}. \tag{5}$$

The rheological model for Casson fluid is defined as

$$\mathrm{T}_{ij} = 2\begin{cases}\left(\mu_{\mathrm{B}} + \dfrac{\mathrm{P}_y}{\sqrt{2\kappa}}\right)m_{ij}, & \kappa > \kappa_c,\\ \left(\mu_{\mathrm{B}} + \dfrac{\mathrm{P}_y}{\sqrt{2\kappa_c}}\right)m_{ij}, & \kappa > \kappa_c.\end{cases} \tag{6}$$

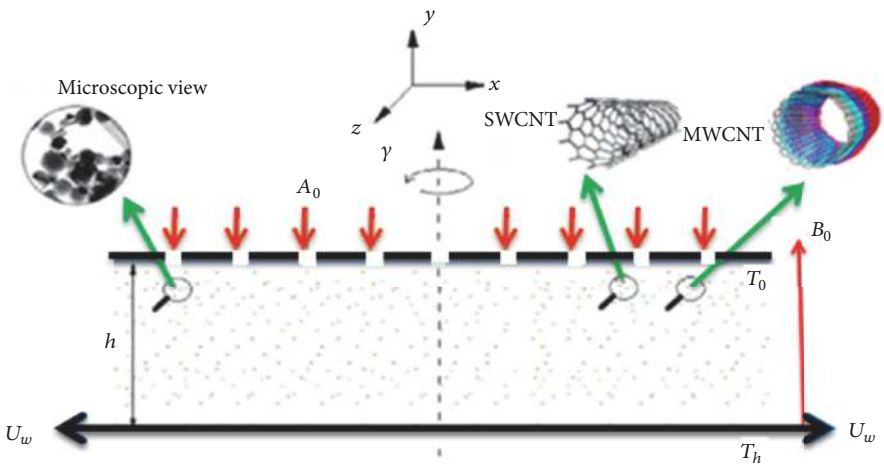

Figure 1: Physical sketch of the problem.

In (1)-(6), $\varphi, f, nf, \mathrm{T}_{ij}, \mu_B, \kappa = m_{ij}$. m_{ij}, P_y, κ_c represent the nanoparticle volume fraction, base fluid, the nanofluid, Cauchy stress tensor, dynamic viscosity, components of strain rate, the yield stress of fluid and the critical value of κ.

3. Mathematical Modeling

Assume the flows of CNTs nanofluid based on kerosene liquid between two parallel (lower and upper) plates which are kept at the distance h. The nanoscale materials (SWCNTs and MWCNTs) are used in this model. The mechanism is examined through the thermal radiation and heat transportation. The constant angular velocity γ rotates around y-axis. The three possible cases $\gamma > 0$ which specify that both upper and lower plates rotated in the same direction $\gamma < 0$ specify that both the plates rotated in opposite directions and $\gamma = 0$ for the static case. The lower plate is moving quickly with a velocity $\mathrm{U}_w = cx$ $(c > 0)$ than the upper plate. A three dimensional coordinate system (x, y, z) is chosen such that x is parallel to the plate, y is normal to the plate, and z is normal to xy-plane. The upper and lower plates are kept at $y = 0$ and $y = h$ respectively. With the help of two opposite forces with same magnitude, the lower plate is being kept stretchable so the position $(0, 0, 0)$ cannot change. The fluid flow and heat transfer is assumed in steady state which is incompressible, laminar, and stable. The magnetic field B_0 is applied in y-direction with which the fluid is rotating as shown in Figure 1 [46].

The governing equations for the state of problem are as follows [46]:

$$\frac{\partial u}{\partial x} + \frac{\partial v}{\partial y} = 0, \tag{7}$$

$$\rho_{nf}\left(u\frac{\partial u}{\partial x} + v\frac{\partial u}{\partial y} + 2\gamma w\right) = -\frac{\partial P^*}{\partial x} + \left(1 + \frac{1}{\beta}\right)\mu_{nf}\left(\frac{\partial^2 u}{\partial x^2} + \frac{\partial^2 u}{\partial y^2}\right) - \sigma_{nf}B_0^2 u, \tag{8}$$

$$\rho_{nf}\left(u\frac{\partial v}{\partial x} + v\frac{\partial v}{\partial y}\right) = -\frac{\partial P^*}{\partial y} + \mu_{nf}\left(1 + \frac{1}{\beta}\right)\left(\frac{\partial^2 v}{\partial x^2} + \frac{\partial^2 v}{\partial y^2}\right), \tag{9}$$

$$\rho_{nf}\left(u\frac{\partial w}{\partial x} + v\frac{\partial w}{\partial y} - 2\gamma u\right) = \mu_{nf}\left(1 + \frac{1}{\beta}\right)\left(\frac{\partial^2 w}{\partial x^2} + \frac{\partial^2 w}{\partial y^2}\right) + \sigma_{nf}B_0^2 w, \tag{10}$$

where $P^* = P - \gamma^2 x^2/2$, σ_{nf} and μ_{nf} represent the modified pressure, electrical conductivity, and dynamic viscosity, respectively. The absenteeism of P_z^* signifies the mesh cross flow beside z-axis and β is the Casson fluid parameter.

The heat transfer phenomenon is specified as [46]:

$$u\frac{\partial \mathrm{T}}{\partial x} + v\frac{\partial \mathrm{T}}{\partial y} = \frac{k_{nf}}{(\rho c)_{nf}}\left(\frac{\partial^2 \mathrm{T}}{\partial x^2} + \frac{\partial^2 \mathrm{T}}{\partial y^2}\right) - \frac{\partial Qr}{\partial y} + \frac{Q_0(T - T_0)}{(\rho c_p)_f}. \tag{11}$$

Here T is the fluid temperature, $\alpha_{nf} = k_{nf}/(\rho c)_{nf}$ is the thermal diffusivity, and Qr is the radiative heat flux, respectively.

The radiative heat flux Qr is defined as

$$Qr = -\frac{4\sigma^*}{3k}\frac{\partial \mathrm{T}^4}{\partial y}, \tag{12}$$

where σ^* and k indicate the absorption coefficient and Stefan Boltzmann constant, respectively.

Since $\mathrm{T}^4 = 4\mathrm{T}_h^3\mathrm{T} - 3\mathrm{T}_h^4$, (11) becomes

$$u\frac{\partial \mathrm{T}}{\partial x} + v\frac{\partial \mathrm{T}}{\partial y} = \frac{k_{nf}}{(\rho c)_{nf}}\left(1 + \frac{16\sigma^*\mathrm{T}_h^3}{3k}\right)\frac{\partial^2 \mathrm{T}}{\partial y^2} + \frac{Q_0(T - T_0)}{(\rho c_p)_f}. \tag{13}$$

The density, heat capacity, dynamic viscosity, and thermal conductivity of the nanofluid are mathematically represented as follows [47–50]:

$$\begin{aligned}
&\rho_{nf} = (1-\varphi)(\rho c)_f + \varphi(\rho c)_{CNT},\\
&(\rho c)_{nf} = (1-\varphi)\rho_f + \varphi\rho_{CNT},\\
&\mu_{nf} = \frac{\mu_f}{(1-\varphi)^{2.5}},\\
&k_{nf}\\
&= k_f\left(\frac{1-\varphi+2\varphi\left(k_{CNT}/k_{CNT-k_f}\right)\ln\left(k_{CNT+k_f}/2k_f\right)}{1-\varphi+2\varphi\left(k_f/k_{CNT-k_f}\right)\ln\left(k_{CNT+k_f}/2k_f\right)}\right).
\end{aligned} \tag{14}$$

where CNT signifies the carbon nanotubes.

T_h is the temperature at lower wall and T_0 is the temperature at upper wall which is taken as $T_h > T_0$.

The above system of equations has the following boundary conditions.

$$\begin{aligned}
&\overrightarrow{u} = U_w = cx,\\
&\overrightarrow{v} = 0,\\
&\overrightarrow{w} = 0,\\
&T = T_h\\
&\qquad\qquad \text{at } y = 0,\\
&\overrightarrow{u} = 0,\\
&\overrightarrow{v} = -A_0,\\
&\overrightarrow{w} = 0,\\
&T = T_0\\
&\qquad\qquad \text{at } y = h.
\end{aligned} \tag{15}$$

In (15), at the upper wall of the channel, A_0 is the uniform suction/injection velocity. If $A_0 > 0$, it is called uniform suction velocity and if $A_0 < 0$, it is called uniform injection velocity.

For the proposed problem we have defined the following similarities variables:

$$\begin{aligned}
&\overrightarrow{u} = cxf'(\xi),\\
&\overrightarrow{v} = -chf(\xi),\\
&\overrightarrow{w} = cxg(\xi),\\
&\theta(\xi) = \frac{T-T_0}{T_h-T_0}, \quad \xi = \frac{y}{h}.
\end{aligned} \tag{16}$$

In view of (8)-(10) and (13), the nondimensional system of equations is

$$\begin{aligned}
&\left(1+\frac{1}{\beta}\right)f^{iv} - (1-\varphi)^{2.5}\left[(1-\varphi)+\varphi\frac{\rho_{CNT}}{\rho_f}\right]\\
&\cdot \mathrm{Re}\left(f'f'' - ff'''\right) - (1-\varphi)^{2.5}\\
&\cdot\left[(1-\varphi)+\varphi\frac{\rho_{CNT}}{\rho_f}\right]\Omega g' - \left(\frac{\sigma_{nf}}{\sigma_f}\right)\mathrm{M}f'' = 0,
\end{aligned} \tag{17}$$

$$\begin{aligned}
&\left(1+\frac{1}{\beta}\right)g'' - (1-\varphi)^{2.5}\left[(1-\varphi)+\varphi\frac{\rho_{CNT}}{\rho_f}\right]\\
&\cdot \mathrm{Re}\left(gf' - fg'\right) + 2(1-\varphi)^{2.5}\left[(1-\varphi)+\varphi\frac{\rho_{CNT}}{\rho_f}\right]\\
&\cdot \Omega f' + \left(\frac{\sigma_{nf}}{\sigma_f}\right)\mathrm{M}g = 0,
\end{aligned} \tag{18}$$

$$\begin{aligned}
&\frac{d}{d\xi}\left(\frac{k_{nf}}{k_f} + Rd\left[1+(\theta-1)\theta\right]^3\right)\theta' + (1-\varphi)^{2.5}\\
&\cdot\left[(1-\varphi)+\varphi\frac{\rho_{CNT}}{\rho_f}\right]\mathrm{Pr}\left(\mathrm{Re}f\theta' - \gamma\theta\right) = 0,
\end{aligned} \tag{19}$$

where the relevant boundary conditions are

$$\begin{aligned}
&f(0) = 0,\\
&f'(0) = 1,\\
&g(0) = 0,\\
&\theta(0) = 1,\\
&f(1) = \varepsilon,\\
&f'(1) = 0,\\
&g(1) = 0,\\
&\theta(1) = 0.
\end{aligned} \tag{20}$$

In (17)-(20), $\varepsilon = A_0/ch$ is the suction and injection parameter. $\varepsilon > 0$ is for the case suction parameter and if $\varepsilon < 0$ is for the case of injection. $\mathrm{Re} = ch^2/\nu_f$ signifies the Reynolds number, $\Omega = \gamma h^2/\nu_f$ represents the rotation parameter, $\mathrm{Pr} = \mu_f c_p/k_f$ signifies the Prandtl number, $Rd = 16\sigma^* T_h^3/3kk^*$ indicates the thermal radiation parameter, $\mathrm{M} = \sigma_f B_0^2 h^2/\rho_f\nu_f$ represents the magnetic parameter, and $\gamma = Q_0/c(\rho c_p)_f$ signifies the heat generation or absorption coefficient.

The equations for the surface drag force and heat transfer rate are defined as follows [51]:

$$\widetilde{C}_f = \left(1+\frac{1}{\beta}\right)\frac{(1-\varphi)^{2.5}}{\left[(1-\varphi)+\varphi\left(\rho_{CNT}/\rho_f\right)\right]}f''(0) \tag{21}$$

$$Nu_x = -\frac{k_{nf}}{k_f}(1+Rd)\theta'(0). \tag{22}$$

4. Expression for Entropy Analysis and Bejan Number

For the stated problem of nanofluid, the local entropy rate $S_{g.t}$ per unit volume is [52]

$$S'''_{g.t} = \frac{k_{nf}}{T_0^2}\left\{(\nabla T)^2 + \frac{16\sigma^* T_h^3}{3kk^*}(\nabla T)^2\right\} + \frac{\mu_{nf}}{T_0}\Phi + \frac{\sigma_{nf}B_0^2}{T_0}\overrightarrow{u}^2, \tag{23}$$

$$S'''_{g.t} = \frac{k_{nf}}{T_0^2}\left\{\left(1 + \frac{16\sigma^* T_h^3}{3k}\right)(\nabla T)^2\right\} + \frac{\mu_{nf}}{T_0}\Phi + \frac{\sigma_{nf}B_0^2}{T_0}\overrightarrow{u}^2, \tag{24}$$

where $(\nabla T) = \mathrm{T}_x + \mathrm{T}_y$ and Φ is related to viscous dissipation.

In our case

$$S'''_{g.t} = \frac{k_{nf}}{T_0^2}\left\{\left(1 + \frac{16\sigma^* T_h^3}{3kk^*}\right)(\nabla T)^2\right\} + \frac{\mu_{nf}}{T_0}\left(\overrightarrow{u}_y\right)^2 + \frac{\sigma_{nf}B_0^2}{T_0}\overrightarrow{u}^2. \tag{25}$$

The characteristic entropy generation rate $S_{g.c}$ is defined as

$$S'''_{g.c} = \frac{k_{nf}(\nabla \mathrm{T})^2}{T_h^2 L^2}. \tag{26}$$

The entropy generation Ns is defined as

$$Ns = \frac{S'''_{g.t}}{S'''_{g.c}}. \tag{27}$$

To calculate the entropy generation Ns, from (25), (26) with (16), implementing in (27), we obtain

$$Ns = \mathrm{Re}\left\{(1 + Rd)\theta'^2 + \frac{1}{(1-\varphi)^{2.5}}\frac{Br}{\omega}\left(f''^2 + M^2 f'^2\right)\right\}, \tag{28}$$

where Re, Br, ω, and M are the Reynolds number, Brinkman number, dimensionless temperature, and Hartmann number, respectively, whose expressions are given by

$$\mathrm{Re} = \mathrm{T}_h^2 L^2, \quad \omega = \frac{\mathrm{T}_h - \mathrm{T}_0}{\mathrm{T}_0}, \quad Br = \frac{\mu_f U_w^2}{k_{nf}(\mathrm{T}_h - \mathrm{T}_0)}. \tag{29}$$

The Bejan number Be is defined as

$$Be = \frac{\left(k_{nf}/\mathrm{T}_0^2\right)\left(1 + 16\sigma^* T_h^3/3kk^*\right)\left(\mathrm{T}_y\right)^2}{\left(\mu_{nf}/\mathrm{T}_0\right)\left(\overrightarrow{u}_y\right)^2 + \left(\sigma_{nf}B_0^2/\mathrm{T}_0\right)\overrightarrow{u}^2}, \tag{30}$$

or

$$Be = \frac{\mathrm{Re}\,(1 + Rd)\,\theta'^2}{\mathrm{Re}\left\{\left(1/(1-\varphi)^{2.5}\right)(Br/\omega)\left(f''^2 + M^2 f'^2\right)\right\}}. \tag{31}$$

5. Solution by HAM

We use homotopy analysis method (HAM) to solve (17)-(19) with (20) by the succeeding process.

The primary assumptions are as follows:

$$f_0(\xi) = \xi + \frac{1}{2}(\varepsilon - 1)\xi^2, \quad \mathrm{g}_0(\xi) = 0, \quad \theta_0(\xi) = 1 - \xi. \tag{32}$$

The linear operators $\mathrm{L}_f, \mathrm{L}_g$, and L_θ are chosen such that

$$L_f(f) = f''', \quad \mathrm{L}_g(\mathrm{g}) = \mathrm{g}'', \quad \mathrm{L}_\theta(\theta) = \theta'', \tag{33}$$

which have the properties

$$L_f\left(b_1 + b_2\xi + b_3\xi^2\right) = 0, \quad \mathrm{L}_g\left(b_4 + b_5\xi\right) = 0, \quad \mathrm{L}_\theta\left(b_6 + b_7\xi\right) = 0, \tag{34}$$

where b_i $(i = 1 \longrightarrow 7)$.

The consequences of nonlinear operators N_f, N_g, and N_θ are indicated as follows:

$$N_f\left[f\left(\xi;'\mathrm{Y}\right), g\left(\xi;'\mathrm{Y}\right)\right] = \left(1 + \frac{1}{\beta}\right)\frac{\partial^4 f\left(\xi;'\mathrm{Y}\right)}{\partial\xi^4} - (1-\varphi)^{2.5}\left[(1-\varphi) + \varphi\frac{\rho_{CNT}}{\rho_f}\right]\mathrm{Re}\left\{\frac{\partial f\left(\xi;'\mathrm{Y}\right)}{\partial\xi}\cdot\frac{\partial^2 f\left(\xi;'\mathrm{Y}\right)}{\partial\xi^2} - f\left(\xi;'\mathrm{Y}\right)\frac{\partial^3 f\left(\xi;'\mathrm{Y}\right)}{\partial\xi^3}\right\} - (1 - \varphi)^{2.5}\left[(1-\varphi) + \varphi\frac{\rho_{CNT}}{\rho_f}\right]\Omega\frac{\partial g\left(\xi;'\mathrm{Y}\right)}{\partial\xi} - \left(\frac{\sigma_{nf}}{\sigma_f}\right)\cdot M\frac{\partial^2 f\left(\xi;'\mathrm{Y}\right)}{\partial\xi^2}, \tag{35}$$

$$N_g\left[f\left(\xi;'\mathrm{Y}\right),g\left(\xi;'\mathrm{Y}\right)\right]=\left(1+\frac{1}{\beta}\right)\frac{\partial^2 g\left(\xi;'\mathrm{Y}\right)}{\partial\xi^2}-(1-\varphi)^{2.5}\left[(1-\varphi)+\varphi\frac{\rho_{CNT}}{\rho_f}\right]\cdot\mathrm{Re}\left(g\left(\xi;'\mathrm{Y}\right)\frac{\partial f\left(\xi;'\mathrm{Y}\right)}{\partial\xi}-f\left(\xi;'\mathrm{Y}\right)\frac{\partial g\left(\xi;'\mathrm{Y}\right)}{\partial\xi}\right)+2\left(1-\varphi\right)^{2.5}\left[\left(1-\varphi\right)+\varphi\frac{\rho_{CNT}}{\rho_f}\right]\Omega\frac{\partial f\left(\xi;'\mathrm{Y}\right)}{\partial\xi}+\left(\frac{\sigma_{nf}}{\sigma_f}\right)Mg\left(\xi;'\mathrm{Y}\right),\tag{36}$$

$$N_\theta\left[f\left(\xi;'\mathrm{Y}\right),\theta\left(\xi;'\mathrm{Y}\right)\right]=\frac{d}{d\xi}\left(\frac{k_{nf}}{k_f}+\frac{4}{3}Rd\right)\left[1+\left(\frac{\partial\theta\left(\xi;'\mathrm{Y}\right)}{\partial\xi}-1\right)\theta\left(\xi;'\mathrm{Y}\right)\right]^3\frac{\partial^2\theta\left(\xi;'\mathrm{Y}\right)}{\partial\xi^2}+\left[\left(1-\varphi\right)+\varphi\frac{\left(\rho c_p\right)_{CNT}}{\left(\rho c_p\right)_f}\right]\cdot\mathrm{Pr}\left(\mathrm{Re}f\left(\xi,'\mathrm{Y}\right)\frac{\partial\theta\left(\xi;'\mathrm{Y}\right)}{\partial\xi}-\gamma\theta\left(\xi;'\mathrm{Y}\right)\right).\tag{37}$$

Zero$^{\text{th}}$-order problems are

$$\left(1-'\mathrm{Y}\right)L_f\left[f\left(\xi;'\mathrm{Y}\right)-f_0\left(\xi\right)\right]='\mathrm{Y}\hbar_f N_f\left[f\left(\xi;'\mathrm{Y}\right),g\left(\xi;'\mathrm{Y}\right)\right],\tag{38}$$

$$\left(1-'\mathrm{Y}\right)L_g\left[g\left(\xi;'\mathrm{Y}\right)-g_0\left(\xi\right)\right]='\mathrm{Y}\hbar_g N_g\left[f\left(\xi;'\mathrm{Y}\right),g\left(\xi;'\mathrm{Y}\right)\right],\tag{39}$$

$$\left(1-'\mathrm{Y}\right)L_\theta\left[\theta\left(\xi;'\mathrm{Y}\right)-\theta_0\left(\xi\right)\right]='\mathrm{Y}\hbar_\theta N_\theta\left[f\left(\xi;'\mathrm{Y}\right),\theta\left(\xi;'\mathrm{Y}\right)\right].\tag{40}$$

The equivalent boundary conditions are

$$\begin{aligned}
f\left(\xi;'\mathrm{Y}\right)\big|_{\xi=0}&=0,\\
\frac{\partial f\left(\xi;'\mathrm{Y}\right)}{\partial\xi}\bigg|_{\xi=0}&=1,\\
f\left(\xi;'\mathrm{Y}\right)\big|_{\xi=1}&=\varepsilon,\\
\frac{\partial f\left(\xi;'\mathrm{Y}\right)}{\partial\xi}\bigg|_{\xi=1}&=0,\\
g\left(\xi;'\mathrm{Y}\right)\big|_{\xi=0}&=0,\\
g\left(\xi;'\mathrm{Y}\right)\big|_{\xi=1}&=0,\\
\theta\left(\xi;'\mathrm{Y}\right)\big|_{\xi=0}&=1,\\
\theta\left(\xi;'\mathrm{Y}\right)\big|_{\xi=1}&=0.
\end{aligned}\tag{41}$$

where $'\mathrm{Y}\in[0,1]$ is the emerging parameter. In case of $'\mathrm{Y}=0$ and $'\mathrm{Y}=1$, we have

$$\begin{aligned}
f\left(\xi;1\right)&=f\left(\xi\right),\\
\mathrm{g}\left(\xi;1\right)&=g\left(\xi\right)\\
\text{and }\theta\left(\xi;1\right)&=\theta\left(\xi\right).
\end{aligned}\tag{42}$$

Expanding $f(\xi;'\mathrm{Y})$, $g(\xi;'\mathrm{Y})$ and $\theta(\xi;'\mathrm{Y})$ by Taylor's series

$$\begin{aligned}
f\left(\xi;'\mathrm{Y}\right)&=f_0\left(\xi\right)+\sum_{q=1}^{\infty}f_q\left(\xi\right)'\mathrm{Y}^q,\\
g\left(\xi;'\mathrm{Y}\right)&=g_0\left(\xi\right)+\sum_{q=1}^{\infty}g_q\left(\xi\right)'\mathrm{Y}^q,\\
\theta\left(\xi;'\mathrm{Y}\right)&=\theta_0\left(\xi\right)+\sum_{q=1}^{\infty}\theta_q\left(\xi\right)'\mathrm{Y}^q,
\end{aligned}\tag{43}$$

where

$$\begin{aligned}
f_q\left(\xi\right)&=\frac{1}{q!}\frac{\partial f\left(\xi;'\mathrm{Y}\right)}{\partial\xi}\bigg|_{'\mathrm{Y}=0},\\
\mathrm{g}_q\left(\xi\right)&=\frac{1}{q!}\frac{\partial g\left(\xi;'\mathrm{Y}\right)}{\partial\xi}\bigg|_{'\mathrm{Y}=0}\\
\text{and }\theta_q\left(\xi\right)&=\frac{1}{q!}\frac{\partial\theta\left(\xi;'\mathrm{Y}\right)}{\partial\xi}\bigg|_{'\mathrm{Y}=0}.
\end{aligned}\tag{44}$$

As the series (44) converges at $'\mathrm{Y}=1$, using $'\mathrm{Y}=1$ in (44), we get

$$\begin{aligned}
f\left(\xi\right)&=f_0\left(\xi\right)+\sum_{q=1}^{\infty}f_q\left(\xi\right),\\
g\left(\xi\right)&=g_0\left(\xi\right)+\sum_{q=1}^{\infty}g_q\left(\xi\right),\\
\theta\left(\xi\right)&=\theta_0\left(\xi\right)+\sum_{q=1}^{\infty}\theta_q\left(\xi\right).
\end{aligned}\tag{45}$$

The q^{th}-order problem gratifies the following:

$$\begin{aligned} L_f\left[f_q(\xi)-\chi_q f_{q-1}(\xi)\right] &= \hbar_f U_q^f(\xi), \\ L_g\left[g_q(\xi)-\chi_q g_{q-1}(\xi)\right] &= \hbar_g U_q^g(\xi), \\ L_\theta\left[\theta_q(\xi)-\chi_q \theta_{q-1}(\xi)\right] &= \hbar_\theta U_q^\theta(\xi). \end{aligned} \tag{46}$$

The equivalent boundary conditions therefore become

$$\begin{aligned} &f_q(0)=f_q'(0)=f_q(1)=f_q'(1)=0, \\ &g_q(0)=g_q(1)=0, \\ &\theta_q(0)=\theta_q(1)=0. \end{aligned} \tag{47}$$

Here

$$\begin{aligned} U_q^f(\xi) &= \left(1+\frac{1}{\beta}\right) f_{q-1}^{iv} - \mathrm{Re}\,(1-\varphi)^{2.5} \\ &\cdot\left[(1-\varphi)+\varphi\frac{\rho_{CNT}}{\rho_f}\right] \\ &\cdot\left(\sum_{k=0}^{q-1} f_{q-1-k}' f_k'' - \sum_{k=0}^{q-1} f_{q-1-k} f_k'''\right) - \Omega\,(1-\varphi)^{2.5} \\ &\cdot\left[(1-\varphi)+\varphi\frac{\rho_{CNT}}{\rho_f}\right] g_{q-1} - \left(\frac{\sigma_{nf}}{\sigma_f}\right) M f_{q-1}'', \end{aligned} \tag{48}$$

$$\begin{aligned} U_q^g(\xi) &= \left(1+\frac{1}{\beta}\right) g_{q-1}'' - (1-\varphi)^{2.5} \\ &\cdot\left[(1-\varphi)+\varphi\frac{\rho_{CNT}}{\rho_f}\right] \\ &\cdot \mathrm{Re}\left(\sum_{k=0}^{q-1} g_{q-1-k} f'_k - \sum_{k=0}^{q-1} f_{q-1-k} g'_k\right) + 2\,(1-\varphi)^{2.5} \\ &\cdot\left[(1-\varphi)+\varphi\frac{\rho_{CNT}}{\rho_f}\right] \Omega f_{q-1}' + \left(\frac{\sigma_{nf}}{\sigma_f}\right) M g_{q-1}, \end{aligned} \tag{49}$$

$$\begin{aligned} U_q^\theta(\xi) &= \frac{d}{d\xi}\left\{\left(\frac{k_{nf}}{k_f}+\frac{4}{3}Rd\right)\left[1+\left(\theta_{q-1}-1\right)\theta_{q-1}\right]^3\right\} \\ &\cdot\theta_{q-1}' + \left[(1-\varphi)+\varphi\frac{(\rho c_p)_{CNT}}{(\rho c_p)_f}\right] \\ &\cdot \mathrm{Pr}\left(\mathrm{Re}\sum_{k=0}^{q-1} f_{q-1-k}\theta_k'' - \gamma\theta_{q-1}\right), \end{aligned} \tag{50}$$

where

$$\chi_q = \begin{cases} 0, & \text{if } {}'\mathrm{Y} \le 1 \\ 1, & \text{if } {}'\mathrm{Y} > 1. \end{cases} \tag{51}$$

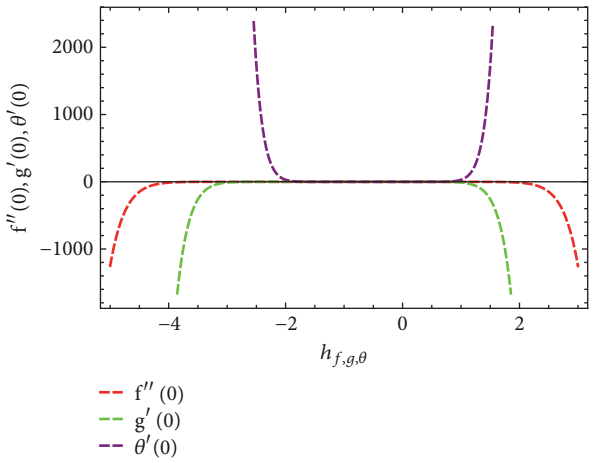

Figure 2: $\hbar$ – curves for $f''(0), g'(0), \theta'(0)$.

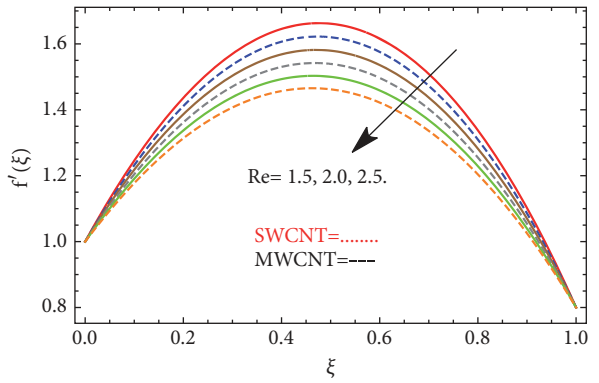

Figure 3: The impact of Re on $f'(\xi)$, when $\varphi = 0.04, A_2 = 0.6, \varepsilon = 0.8, \beta = 0.7, M = 1.0$.

5.1. HAM Solution Convergence. The assisting parameters $\hbar_f, \hbar_g$, and $\hbar_\theta$ appear when we calculate the series solution of velocities ($f'(\xi), g(\xi)$) and temperature ($\theta(\xi)$) functions by using HAM. These parameters lead the convergence of the modeled problem. Figure 2 is schemed to see the convergence of the problem. The velocity function $f'(\xi)$ converges in the region $-4.0 \le \hbar_f \le 2.0$, the velocity function $g(\xi)$ converges in the region $-3.0 \le \hbar_g \le 1.0$, and the temperature function $\theta(\xi)$ converges in the region $-2.0 \le \hbar_\theta \le 1.0$, respectively.

6. Results and Discussion

To discuss the impact of embedded parameters on velocities $f'(\xi), g(\xi)$, temperature $\theta(\xi)$, entropy generation rate (Ns), and Bejan numbers (Be), Figures 3–21 are plotted. These parameters are Reynolds number (Re), Rotation parameter (Ω), magnetic parameter (M), Casson parameter (β), Prandtl number (Pr), thermal radiation parameter (Rd), and heat source/sink (γ). Figure 1 shows physical shape of the nanofluid flow. Figure 2 is plotted to see the convergence region of modeled problem.

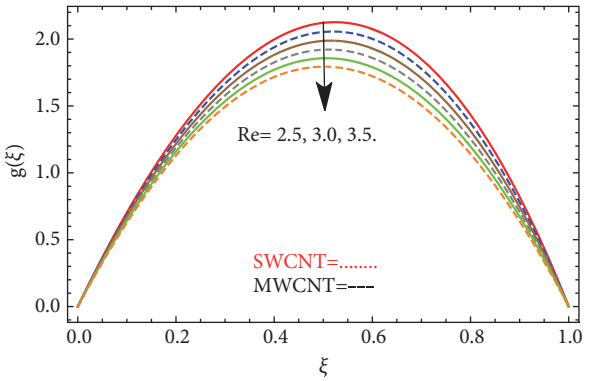

FIGURE 4: The impact of Re on $g(\xi)$, when $\varphi = 0.04, \Omega = 0.6, \beta = 0.7, M = 1.0$.

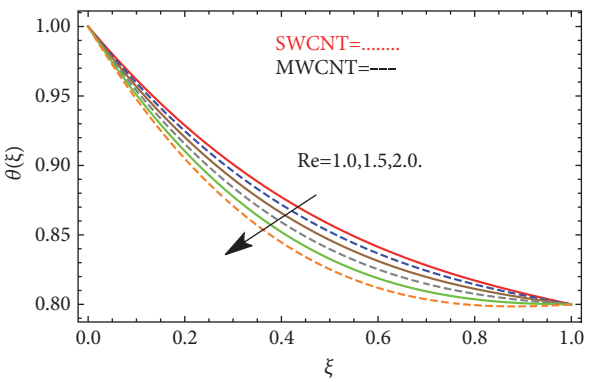

FIGURE 5: The impact of Re on $\theta(\xi)$, when $\varphi = 0.04, \mathrm{Pr} = 7.1, \gamma = 0.8, Rd = 0.9, M = 1.0$.

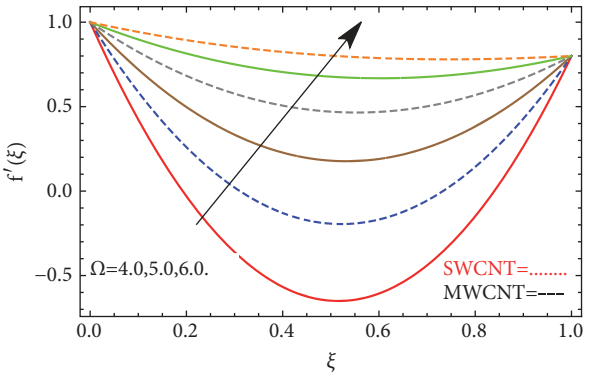

FIGURE 6: The impact of Ω on $f'(\xi)$, when $\varphi = 0.04, \mathrm{Re} = 0.5, \varepsilon = 0.8, \beta = 0.7, M = 1.0$.

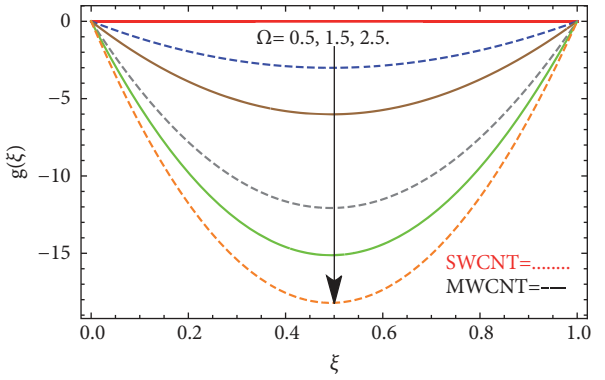

FIGURE 7: The impact of Ω on $g(\xi)$, when $\varphi = 0.04, \mathrm{Re} = 0.5, M = 1.0, \beta = 0.7$.

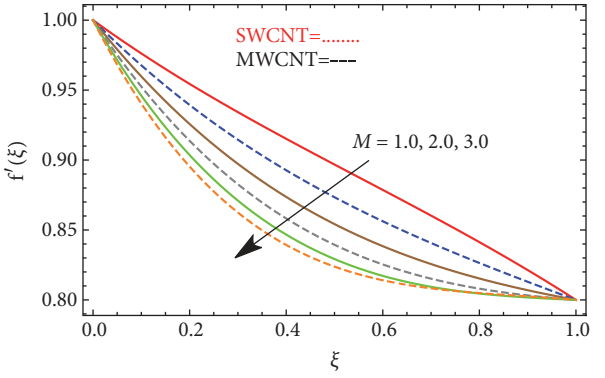

FIGURE 8: The impact of M on $f'(\xi)$, when $\varphi = 0.04, \mathrm{Re} = 0.5, \Omega = 0.6, \beta = 0.7, \varepsilon = 0.8$.

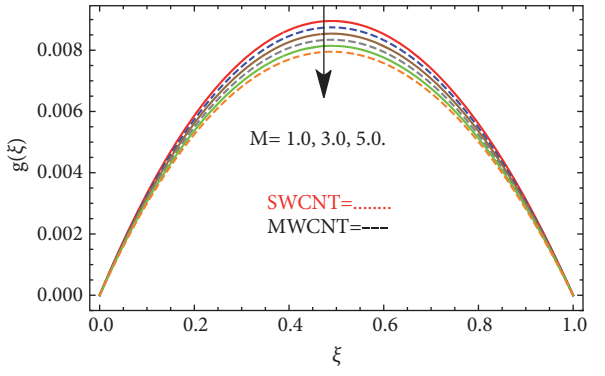

FIGURE 9: The impact of M on $g(\xi)$, when $\varphi = 0.04, \mathrm{Re} = 0.5, \Omega = 0.6, \beta = 0.7$.

6.1. Velocities and Temperature Profiles. Figures 3–5 are plotted to observe the effect of (Re) on ($f'(\xi)$ and $g(\xi)$) and $\theta(\xi)$. Reynolds is a dimensionless number used to calculate the flow pattern in different situation of the fluid flow. At low Reynolds numbers, the fluid flow tends to laminar while at low Reynolds numbers, the fluid flow tends to turbulent flow. From here, we observed that with the escalating values of (Re) the velocities ($f'(\xi)$ and $g(\xi)$) and temperature $\theta(\xi)$ profiles decrease. This is due to the stretching of the lower plate. The effect of (Ω) on velocities ($f'(\xi)$ and $g(\xi)$) profiles is shown in Figures 6-7. From Figure 6, we observed the increasing behavior with the increasing rotation parameter while the opposite result was observed in Figure 7. It is interesting to mention that in the absence of rotation parameter the problem reduces to 2-dimensional flow in a channel. Figures 8-9 are plotted to observe the impact of (M) parameter on velocities ($f'(\xi)$ and $g(\xi)$) profiles. According

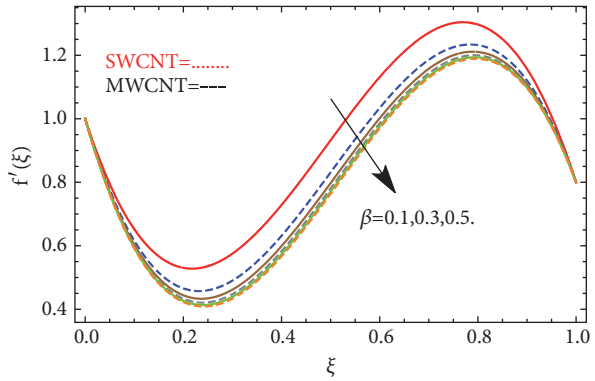

FIGURE 10: The impact of (β) on $f'(\xi)$, when $\varphi = 0.04$, Re $= 0.5$, $\Omega = 0.6$, $M = 1.0$.

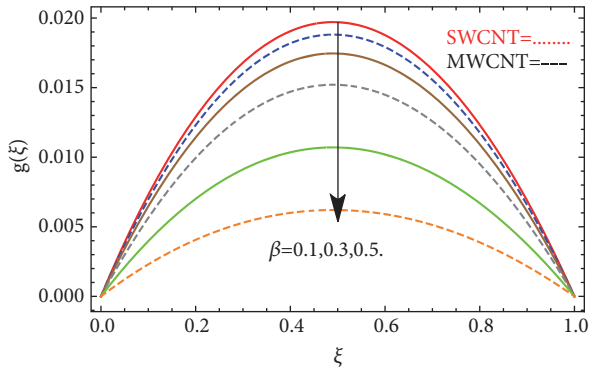

FIGURE 11: The impact of β on $g(\xi)$, when $\varphi = 0.04$, Re $= 0.5$, $\Omega = 0.6$.

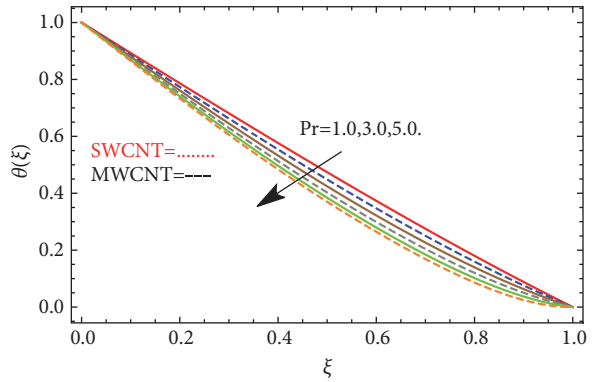

FIGURE 12: The impact of Pr on $\theta(\xi)$, when $\varphi = 0.04$, Re $= 0.5$, $\gamma = 0.8$, $Rd = 0.9$.

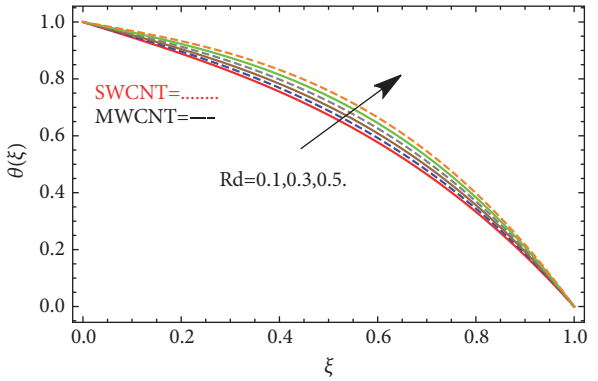

FIGURE 13: The impact of Rd on $\theta(\xi)$, when $\varphi = 0.04$, Re $= 0.5$, $\gamma = 0.8$, Pr $= 0.9$.

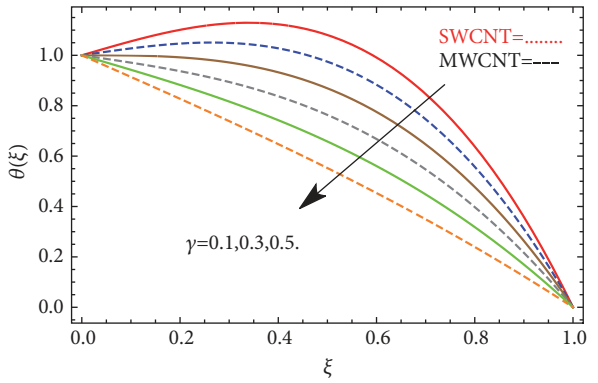

FIGURE 14: The impact of γ on $\theta(\xi)$, when $\varphi = 0.04$, Re $= 0.5$, $Rd = 0.8$, Pr $= 0.9$.

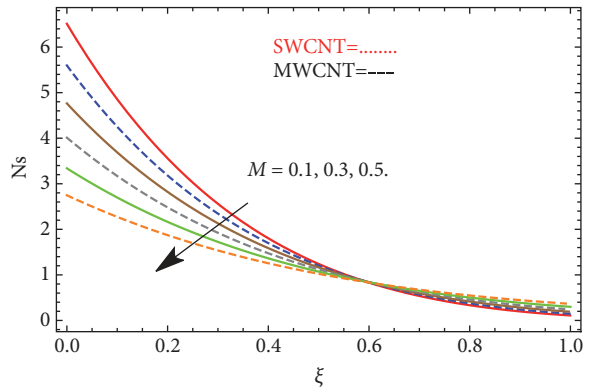

FIGURE 15: The impact of M on Ns, when $\varphi = 0.04$, $Rd = 0.9$, $\omega = 0.5$, $Br = 0.25$, Re $= 1.0$.

to Lorentz force theory, the magnetic field parameter has an inverse effect on $(f'(\xi)$ and $g(\xi))$ profiles, that is, the upsurges in magnetic field parameter the $(f'(\xi)$ and $g(\xi))$ profiles reduce. Figures 10-11 depict the impact of (β) on $(f'(\xi)$ and $g(\xi))$ profiles. In practice, the increasing (β) results in the rise in dynamic viscosity that creates a resistance in the flow and a decline in fluid velocity thereof. Therefore, the increasing in Casson fluid parameter reduces the velocities $(f'(\xi)$ and $g(\xi))$ profiles. Figure 12 is schemed to observe the influence of (Pr) on temperature profile $\theta(\xi)$. Physically, nanofluids have large thermal diffusivity with small (Pr) and vice versa. Therefore, the liquid temperature decreases. From here we observed that the growing (Pr) shows decline in $\theta(\xi)$. Figure 13 is schemed to observe the impact of (Rd) on $\theta(\xi)$. Thermal radiations have leading rules in heat transmission, when the coefficient of convection heat transmission is small. From here we observed that the increasing (Rd) shows a rapid

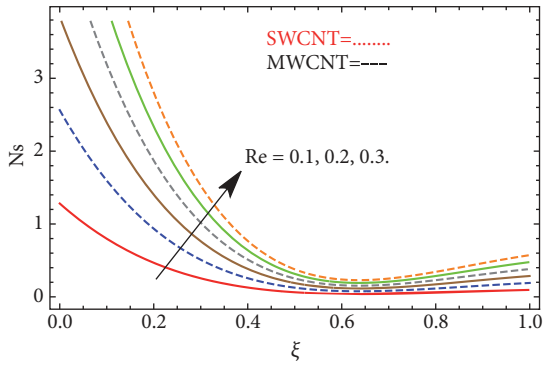

Figure 16: The impact of Re on Ns, when $\varphi = 0.04, Rd = 0.9, \omega = 0.5, Br = 0.25, M = 1.0$.

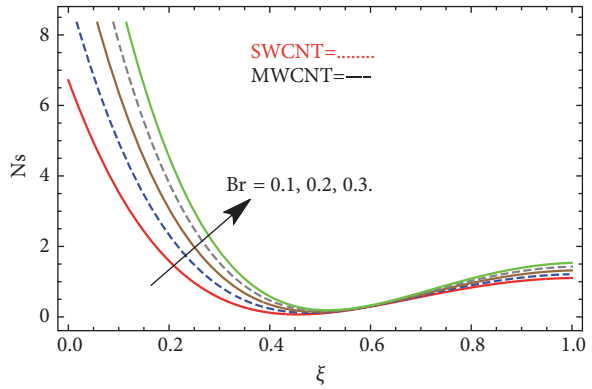

Figure 17: The impact of Br on Ns, when $\varphi = 0.04, Rd = 0.9, \omega = 0.5, M = 0.25, \mathrm{Re} = 1.0$.

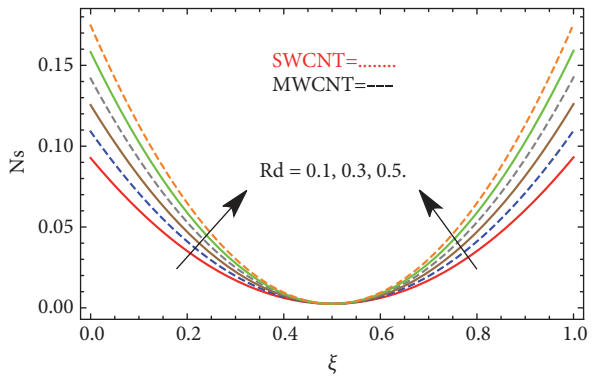

Figure 18: The impact of Rd on Ns, when $\varphi = 0.04, \mathrm{Re} = 1.0, \omega = 0.5, Br = 0.5, M = 0.25$.

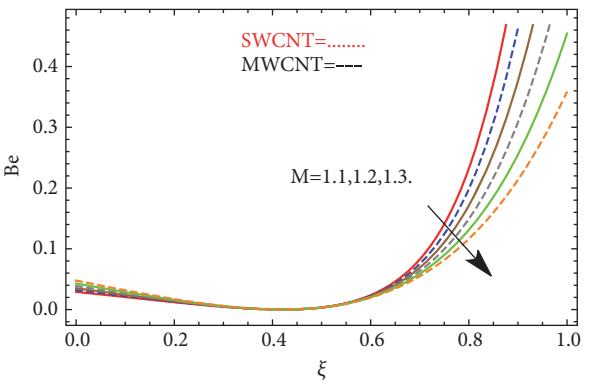

Figure 19: The impact of M on Be, when $\varphi = 0.04, Rd = 0.9, \omega = 0.5, Br = 0.25$.

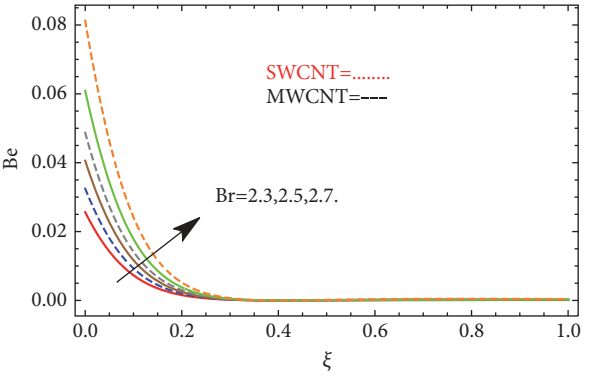

Figure 20: The impact of Br on Be, when $\varphi = 0.04, Rd = 0.9, \omega = 0.5, M = 0.25$.

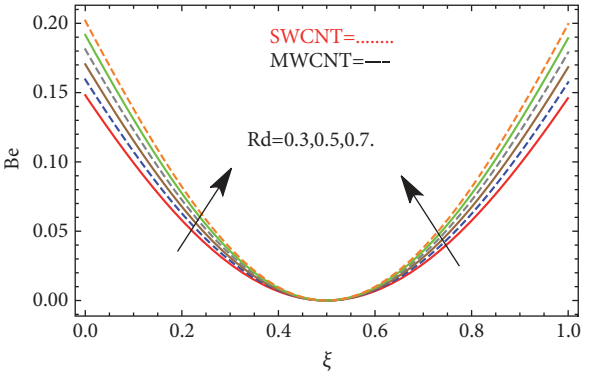

Figure 21: The impact of Rd on Be, when $\varphi = 0.04, Br = 0.25, \omega = 0.5, M = 0.25$.

increase in $\theta(\xi)$. Figure 14 specifies the impact of (γ) on $\theta(\xi)$. The porosity parameter has commanding character in fluid motion. Physically, the higher values of porosity parameter improve the porous surface which resists to the flow motion and as a result the motion of the fluid reduces. From here we see that $\theta(\xi)$ decreases with increasing (γ).

6.2. Entropy Generation and Bejan Number. Figures 15–21 are plotted to see the influences of emerging parameters for both SWCNTs and MWCNTs based on kerosene nanoliquids on entropy generation Ns and Bejan number (Be). Generally, the entropy generation rate is more for SWCNTs as compared to MWCNTs. Figure 15 shows the impact of (M) on (Ns). Physically, due to magnetic parameter Lorentz force generates and decreases velocity of the flow and thus entropy generation declines. Figure 16 expresses the impact of (Re) on (Ns). With high Reynolds number, hectic motion arises for the reason that as (Re) escalates, the fluid moves more upsettingly and

Table 1: The arithmetical values of surface drag force $\widetilde{C}_f = (\mu_{nf}/\mu_f) f''(0)$, when $\sigma = 0.04$.

Re	Ω	M	β	$\widetilde{C}_f$
0.1	0.2	0.3	1.0	-0.524696
0.2				-0.521175
0.3	0.3			-0.520833
	0.4			-0.497588
	0.5	0.3		-0.507138
		0.5		-0.515129
		1.0	1.0	-0.526225
			1.1	-0.516946
			1.2	-0.509188

Table 2: The arithmetical values of heat transfer rate $Nu_x = (-k_{nf}/k_f)(1 + Rd)\theta'(0)$, when $\sigma = 0.04$.

Re	Pr	Rd	γ	Nu_x
0.1	7.1	0.1	0.1	-0.001095
0.2				-0.001094
0.3	7.1			-0.001091
	7.2			-0.001095
	7.3	0.1		-0.001099
		0.2		-0.001103
		0.3	0.1	-0.001349
			0.2	0.209913
			0.3	0.214909

Table 3: Physical properties of CNTs [45].

Materials	SWCNT	MWCNT
Thermal Conductivity k_{nf} W/mK	1×10^3	1×10^3
Electrical Conductivity φ_{nf} S/m	$1 \times 10^6 - 1 \times 10^7$	$1 \times 10^6 - 1 \times 10^7$
Tensile Strength (GPa)	1.5×10^2	1.5×10^2
Young's Modulus (GPa)	10.54×10^2	1.2×10^3

hence contribution of the fluid fraction and heat transfer on entropy result tends to escalation in entropy generation rate. Figure 17 shows the influence of (Br) on (Ns). The entropy generation rate escalates with the escalation in (Br). In addition, an increase in (Ns) created by fluid friction and joule dissipation happens with the escalating values of (Br). Figure 18 shows the influence of (Rd) on (Ns). From the figure we see that at $0.0 \leq \xi < 0.5$ and $0.5 < \xi \leq 1.0$ the escalating values of (Rd) show increasing behavior in (Ns). But at the mean position (i-e $\xi = 0.5$), the radiation parameter has no impact on (Ns). It is due to the stretching of the lower plate. Figure 19 shows the influence of (M) on (Be). It is clear from the figures that the accelerating values of (M) shows decline in (Be). Figure 20 depicts the influence of (Br) on (Be). The increasing values of (Br) escalate the (Be). Figure 21 indicates the influence of (Rd) on (Be). From the figure we see that at $0.0 \leq \xi < 0.5$ and $0.5 < \xi \leq 1.0$ the increasing values of (Rd) show increasing behavior in (Be), while at $\xi = 0.5$ the radiation parameter does not show increasing or decreasing behavior. It is due to the stretching of the lower plate.

6.3. Tables Discussion. Table is schemed to observe the impact of (Re), (Ω), (M), and (β) on skin fraction coefficient $\widetilde{C}_f$. From Table 1, we observed that the surface drag force increases with the escalation in (Re) and (β) while it reduces with the escalation in (Ω) and (M). Table 2 is schemed to observe the impact of (Re), (Rd), (Pr), and (γ) on local Nusselt number Nu_x. From here it is observed that the heat transfer rate increases with the escalation in (Re) and (γ) while it reduces with the escalation in (Rd) and (Pr). In Tables 3–5, some physical and thermal properties of CNTs with thermal conductivity are presented.

Table 4: The thermophysical properties of CNTs and nanofluids of some base fluids [53].

Physical Properties		Specific Heat $c_p(J/kgK)$	Density $\rho(kg/m^3)$	Thermal Conductivity $k(W/mk)$
Base fluid	Water	41.97×10^2	0.997×10^3	61.3×10^{-2}
	Kerosene (lamp) oil	20.90×10^2	0.783×10^3	14.5×10^{-2}
	Engine oil	19.10×10^2	0.884×10^3	14.4×10^{-2}
Nanofluids	SWCNT	0.425×10^3	2.6×10^3	6.6×10^3
	MWCNT	0.796×10^3	1.6×10^3	30×10^2

Table 5: Thermal conductivity (k_{nf}) of CNTs with different volume fraction (φ).

φ	k_{nf} for SWCNT	k_{nf} for MWCNT
0	14.5×10^{-2}	14.5×10^{-2}
0.01	17.4×10^{-2}	17.2×10^{-2}
0.02	20.4×10^{-2}	2×10^{-1}
0.03	23.5×10^{-2}	22.8×10^{-2}
0.04	26.6×10^{-2}	25.7×10^{-2}

7. Conclusion

Entropy generation examination in two-dimensional mixed convection flow of nanofluid over an inclined stretching sheet has been analyzed. The kerosene liquid is taken as base fluid. The impact of magnetohydrodynamics, thermal radiation, and heat/source has been examined. The transformed system of equations has been solved by homotopy analysis method. On the achieved study, the key remarks are listed below.

(i) The velocity function $f'(\xi)$ escalates with the escalation in rotation parameter and reduces with rise in Reynolds number, magnetic field parameter, and Casson fluid parameter.

(ii) The velocity function $g(\xi)$ is reduced with escalation in Reynolds number, rotation parameter, magnetic field, and Casson fluid parameter.

(iii) The temperature function $\theta(\xi)$ is increased with the escalation in thermal radiation parameter while reduced with the escalation in Reynolds number, Prandtl number, and heat source/sink.

(iv) The entropy generation Ns is increased with the escalation in Reynolds number, Brinkman number, and thermal radiation parameter while reduced with the escalation in magnetic field parameter.

(v) The Bejan number is increased with the increase in Brinkman number and thermal radiation parameter while reduced with the upsurge in magnetic field parameter.

(vi) The surface drag force increases with the escalation in Reynolds number and Casson fluid parameter while reduces with the escalation in rotation and magnetic parameter.

(vii) The heat transfer rate increases with the escalation in Reynolds number and heat source/sink while reduces with the escalation in thermal radiation parameter and Prandtl number.

Nomenclature

$b_1, b_2, b_3, b_4, b_5, b_6, b_7$: Constants
A_0: Suction/injection
B_0: Magnetic field (NmA^{-1})
c_p: Specific heat (J/kgK)
$\widetilde{C}_f$: Skin friction coefficient
h: Distance between the plates (m)
k: Thermal conductivity ($Wm^{-1}K^{-1}$)
k^*: Stefan Boltzmann constant
Ω: Rotation parameter
Nu: Nusselt number
O: Origen
P^*: Fluid pressure (Pa)
P_z^*: Mesh cross flow
Pr: Prandtl number
Q_0: Heat flux (Wm^{-2})
Q_r: Radioactive heat flux (J)
Rd: Radiation parameter
T: Fluid temperature (K)
T_0: Temperature at upper wall
T_h: Temperature at lower wall
u, v: Velocity components (ms^{-1})
U_w: Stretching velocity (ms^{-1})
x, y, z: Coordinates

Greek Letters

β: Casson parameter
γ: Angular velocity
α_{nf}: Thermal diffusivity (m^2s^{-1})
ξ: Similarity variable
μ_{nf}: Dynamic viscosity (mPa)
ρ_{nf}: Base fluid density (Kgm^{-3})
σ_{nf}: Electrical conductivity of nanofluid (Sm^{-1})
φ: Nanoparticle volume fraction
σ^*: Absorption coefficient
$\hbar$: Assisting parameter.

Data Availability

The data used to support the findings of this study are available from the corresponding author upon request.

Conflicts of Interest

The authors declare that they have no conflicts of interest.

References

[1] C. Sus, "Enhancing thermal conductivity of fluids with nanoparticles," *International Mechanical Engineering Congress and Exposition*, vol. 66, pp. 99–105, 1995.

[2] R. Ul Haq, S. Nadeem, Z. H. Khan, and N. F. M. Noor, "Convective heat transfer in MHD slip flow over a stretching surface in the presence of carbon nanotubes," *Physica B: Condensed Matter*, vol. 457, pp. 40–47, 2015.

[3] M. S. Liu, M. Ching-Cheng Lin, I. T. Huang, and C. C. Wang, "Enhancement of thermal conductivity with carbon nanotube for nanofluids," *International Communications in Heat and Mass Transfer*, vol. 32, no. 9, pp. 1202–1210, 2005.

[4] S. Nadeem and C. Lee, "Boundary layer flow of nanofluid over an exponentially stretching surface," *Nanoscale Research Letters*, vol. 94, no. 7, 2012.

[5] R. Ellahi, M. Raza, and K. Vafai, "Series solutions of non-Newtonian nanofluids with Reynolds' model and Vogel's model by means of the Homotopy analysis method," *Mathematical and Computer Modelling*, vol. 55, no. 7-8, pp. 1876–1891, 2012.

[6] S. Nadeem, R. U. Haq, and Z. H. Khan, "Numerical study of MHD boundary layer flow of a Maxwell fluid past a stretching sheet in the presence of nanoparticles," *Journal of the Taiwan Institute of Chemical Engineers*, vol. 45, no. 1, pp. 121–126, 2014.

[7] S. Nadeem and R. Ul Haq, "MHD boundary layer flow of a nanofluid past a porous shrinking sheet with thermal radiation," *Journal of Aerospace Engineering*, vol. 28, no. 2, Article ID 04014061, 2015.

[8] S. Nadeem and R. Ul Haq, "Effect of thermal radiation for megnetohydrodynamic boundary layer flow of a nanofluid past a stretching sheet with convective boundary conditions," *Journal of Computational and Theoretical Nanoscience*, vol. 11, no. 1, pp. 32–40, 2014.

[9] J. Buongiorno, "Convective transport in nanofluids," *Journal of Heat Transfer*, vol. 128, no. 3, pp. 240–250, 2006.

[10] M. Sheikholeslami, Z. Shah, A. Shafee, I. Khan, and I. Tlili, "Uniform magnetic force impact on water based nanofluid thermal behavior in a porous enclosure with ellipse shaped obstacle," *Scientific Reports*, vol. 9, 2019.

[11] M. Sheikholeslami, "Magnetic field influence on nanofluid thermal radiation in a cavity with tilted elliptic inner cylinder," *Journal of Molecular Liquids*, vol. 229, pp. 137–147, 2017.

[12] M. Sheikholeslami, Z. Shah, A. Tassaddiq, A. Shafee, and I. Khan, "Application of electric field for augmentation of ferrofluid heat transfer in an enclosure with double moving walls," *IEEE Access*, vol. 7, pp. 21048–21056, 2019.

[13] M. Sheikholeslami, "Numerical simulation of magnetic nanofluid natural convection in porous media," *Physics Letters A*, vol. 381, no. 5, pp. 494–503, 2017.

[14] M. Sheikholeslami, "Numerical study of heat transfer enhancement in a pipe filled with porous media by axisymmetric TLB model based on GPU," *The European Physical Journal Plus*, vol. 129, article 248, 2014.

[15] M. Sheikholeslami, "CVFEM for magnetic nanofluid convective heat transfer in a porous curved enclosure," *The European Physical Journal Plus*, vol. 131, no. 413, 2016.

[16] M. Sheikholeslami and H. B. Rokni, "Simulation of nanofluid heat transfer in presence of magnetic field: A review," *International Journal of Heat and Mass Transfer*, vol. 115, pp. 1203–1233, 2017.

[17] M. Sheikholeslami and H. B. Rokni, "Free convection of CuOeH2O nanofluid in a curved porous enclosure using mesoscopic approach," *International Journal of Hydrogen Energy*, vol. 42, article 15393, 2017.

[18] M. Sheikholeslami and H. B. Rokni, "Numerical simulation for impact of Coulomb force on nanofluid heat transfer in a porous enclosure in presence of thermal radiation," *International Journal of Heat and Mass Transfer*, vol. 118, pp. 823–831, 2018.

[19] M. Sheikholeslami, D. Domiri Ganji, M. Younus Javed, and R. Ellahi, "Effect of thermal radiation on magnetohydrodynamics nanofluid flow and heat transfer by means of two phase model," *Journal of Magnetism and Magnetic Materials*, vol. 374, pp. 36–43, 2015.

[20] M. M. Elias, M. Miqdad, I. M. Mahbubul et al., "Effect of nanoparticle shape on the heat transfer and thermodynamic performance of a shell and tube heat exchanger," *International Communications in Heat and Mass Transfer*, vol. 44, pp. 93–99, 2013.

[21] H. Alfvén, "Existence of electromagnetic-hydrodynamic waves," *Nature*, vol. 150, no. 3805, pp. 405-406, 1942.

[22] T. Hayat, S. A. Shehzad, and A. Alsaedi, "Soret and Dufour effects on magnetohydrodynamic (MHD) flow of Casson fluid," *Applied Mathematics and Mechanics-English Edition*, vol. 33, no. 10, pp. 1301–1312, 2012.

[23] F. Ali, N. A. Sheikh, I. Khan, and M. Saqib, "Magnetic field effect on blood flow of Casson fluid in axisymmetric cylindrical tube: a fractional model," *Journal of Magnetism and Magnetic Materials*, vol. 423, pp. 327–336, 2017.

[24] Z. Shah, T. Gul, A. M. Khan, I. Ali, and S. Islam, "Effects of hall current on steady three dimensional non-newtonian nanofluid in a rotating frame with brownian motion and thermophoresis effects," *Journal of Engineering and Technology*, vol. 6, pp. 280–296, 2017.

[25] Z. Shah, S. Islam, T. Gul, E. Bonyah, and M. Altaf Khan, "The electrical MHD and Hall current impact on micropolar nanofluid flow between rotating parallel plates," *Results in Physics*, vol. 9, pp. 1201–1214, 2018.

[26] Z. Shah, T. Gul, S. Islam et al., "Three dimensional third grade nanofluid flow in a rotating system between parallel plates with Brownian motion and thermophoresis effects," *Results in Physics*, vol. 10, pp. 36–45, 2018.

[27] A. Dawar, Z. Shah, W. Khan, M. Idrees, and S. Islam, "Unsteady squeezing flow of magnetohydrodynamic carbon nanotube nanofluid in rotating channels with entropy generation and viscous dissipation," *Advances in Mechanical Engineering*, vol. 11, no. 1, 2019.

[28] K. A. Kumar, J. V. Reddy, V. Sugunamma, and N. Sandeep, "Simultaneous solutions for MHD flow of williamson fluid over a curved sheet with nonuniform heat source/sink," *Heat Transfer Research*, vol. 50, no. 6, pp. 581–603, 2019.

[29] G. Kumaran and N. Sandeep, "Thermophoresis and Brownian moment effects on parabolic flow of MHD Casson and Williamson fluids with cross diffusion," *Journal of Molecular Liquids*, vol. 233, pp. 262–269, 2017.

[30] K. Anantha Kumar, V. Sugunamma, N. Sandeep, and J. V. Ramana Reddy, "Impact of Brownian motion and thermophoresis on bioconvective flow of nanoliquids past a variable thickness surface with slip effects," *Multidiscipline Modeling in Materials and Structures*, vol. 15, no. 1, 2018.

[31] A. K. Kumar, S. Vangala., and N. Sandeep, "Impact of nonlinear radiation on MHD non-aligned stagnation point flow of micropolar fluid over a convective surface," *Journal of Non-Equilibrium Thermodynamics*, vol. 43, no. 4, pp. 327–345, 2018.

[32] K. Anantha Kumar, B. Ramadevi, and V. Sugunamma, "Impact of lorentz force on unsteady bio convective flow of carreau fluid across a variable thickness sheet with non-fourier heat flux model," *Defect and Diffusion Forum*, vol. 387, pp. 474–497, 2018.

[33] K. A. Kumar, J. V. Ramana Reddy, S. Vangala, and N. Sandeep, "MHD flow of chemically reacting Williamson fluid over a curved/flat surface with variable heat source/sink," *International Journal of Fluid Mechanics Research*.

[34] K. A. Kumar, J. V. Ramana Reddy, S. Vangala, and N. Sandeep, "Magnetohydrodynamic Cattaneo-Christov flow past a cone and a wedge with variable heat source/sink," *Alexandria Engineering Journal*, vol. 57, pp. 435–443, 2018.

[35] K. Anantha Kumar, J. V. Ramana Reddy, V. Sugunamma, and N. Sandeep, "Impact of cross diffusion on MHD viscoelastic fluid flow past a melting surface with exponential heat source," *Multidiscipline Modeling in Materials and Structures*, vol. 14, no. 5, pp. 999–1016, 2018.

[36] B. Ramadevi, V. Sugunamma, K. Anantha Kumar, and J. V. Ramana Reddy, "MHD flow of Carreau fluid over a variable thickness melting surface subject to Cattaneo-Christov heat flux," *Multidiscipline Modeling in Materials and Structures*, vol. 15, no. 1, 2018.

[37] Z. Mehmood, R. Mehmood, and Z. Iqbal, "Numerical investigation of micropolar Casson fluid over a stretching sheet with internal heating," *Communications in Theoretical Physics*, vol. 67, no. 4, pp. 443–448, 2017.

[38] Z. Iqbal, R. Mehmood, E. Azhar, and Z. Mehmood, "Impact of inclined magnetic field on micropolar Casson fluid using Keller box algorithm," *The European Physical Journal Plus*, vol. 132, no. 175, 2017.

[39] A. M. Megahed, "Effect of slip velocity on Casson thin film flow and heat transfer due to unsteady stretching sheet in presence of variable heat flux and viscous dissipation," *Open Journal of Fluid Dynamic*, vol. 6, pp. 303–306, 2015.

[40] M. H. Abolbashari, N. Freidoonimehr, F. Nazari, and M. M. Rashidi, "Analytical modeling of entropy generation for Casson nano-fluid flow induced by a stretching surface," *Advanced Powder Technology*, vol. 26, no. 2, pp. 542–552, 2015.

[41] J. C. Maxwell, *Electricity and Magnetism*, Clarendon, Oxford, 3rd edition, 1904.

[42] D. J. Jeffrey, "Conduction through a random suspension of spheres," *Proceedings of the Royal Society A Mathematical, Physical and Engineering Sciences*, vol. 335, no. 1602, pp. 355–367, 1973.

[43] R. H. Davis, "The effective thermal conductivity of a composite material with spherical inclusions," *International Journal of Thermophysics*, vol. 7, no. 3, pp. 609–620, 1986.

[44] R. L. Hamilton and O. K. Crosser, "Thermal conductivity of heterogeneous two-component systems," *Industrial & Engineering Chemistry Fundamentals*, vol. 1, no. 3, pp. 187–191, 1962.

[45] Q. Z. Xue, "Model for thermal conductivity of carbon nanotube-based composites," *Physica B: Condensed Matter*, vol. 368, no. 1-4, pp. 302–307, 2005.

[46] Z. Shah, A. Dawar, S. Islam, I. Khan, and D. L. Ching, "Darcy-Forchheimer flow of radiative carbon nanotubes with microstructure and inertial characteristics in the rotating frame," *Case Studies in Thermal Engineering*, vol. 12, pp. 823–832, 2018.

[47] A. Dawar, Z. Shah, S. Islam, M. Idress, and W. Khan, "Magnetohydrodynamic CNTs casson nanofluid and radiative heat transfer in a rotating channels," *Journal of Physics Research and Applications*, vol. 1, pp. 017–032, 2018.

[48] N. Nasir, Z. Shah, S. Islam, E. Bonyah, and T. Gul, "Darcy forchheimer nanofluid thin film flow of SWCNTs and heat transfer analysis over an unsteady stretching sheet," *AIP Advances*, vol. 9, Article ID 015223, 2019.

[49] Z. Shah, E. Bonyah, S. Islam, and T. Gul, "Impact of thermal radiation on electrical MHD rotating flow of Carbon nanotubes over a stretching sheet," *AIP Advances*, vol. 9, no. 1, Article ID 015115, 2019.

[50] A. Ali, M. Sulaiman, S. Islam, Z. Shah, and E. Bonyah, "Three-dimensional magnetohydrodynamic (MHD) flow of Maxwell nanofluid containing gyrotactic micro-organisms with heat source/sink," *AIP Advances*, vol. 8, Article ID 085303, 2018.

[51] Z. Shah, E. Bonyah, S. Islam, W. Khan, and M. Ishaq, "Radiative MHD thin film flow of Williamson fluid over an unsteady permeable stretching sheet," *Heliyon*, vol. 4, no. 10, Article ID e00825, 2018.

[52] M. Jawad, Z. Shah, S. Islam, E. Bonyah, and A. Z. Khan, "Darcy-forchheimer flow of MHD nanofluid thin film flow with Joule dissipation and Navier's partial slip," *Journal of Physics Communications*, vol. 2, no. 11, p. 115014, 2018.

[53] M. Jawad, Z. Shah, S. Islam et al., "Impact of nonlinear thermal radiation and the viscous dissipation effect on the unsteady three-dimensional rotating flow of single-wall carbon nanotubes with aqueous suspensions," *Symmetry*, vol. 11, no. 2, article 207, 2019.

[54] S. Alharbi, A. Dawar, Z. Shah et al., "Entropy generation in MHD eyring–powell fluid flow over an unsteady oscillatory porous stretching surface under the impact of thermal radiation and heat source/sink," *Applied Sciences*, vol. 8, no. 12, article 2588, 2018.

[55] N. Khan, Z. Shah, S. Islam, I. Khan, T. Alkanhal, and I. Tlili, "Entropy generation in MHD mixed convection non-newtonian second-grade nanoliquid thin film flow through a porous medium with chemical reaction and stratification," *Entropy*, vol. 21, no. 2, article 139, 2019.

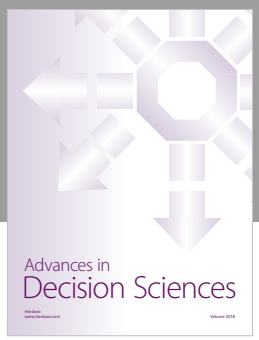

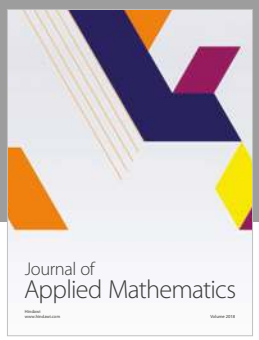

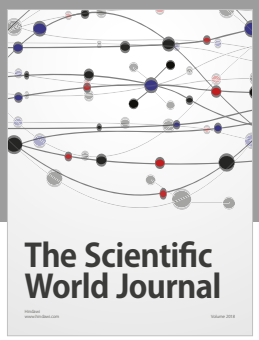

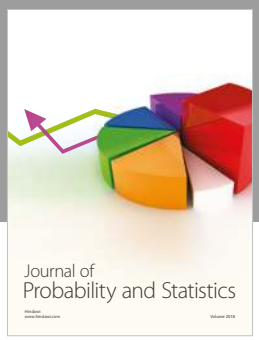

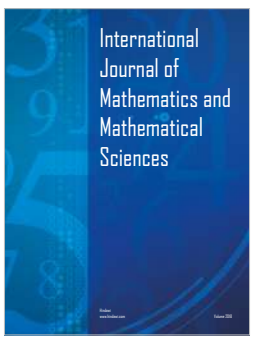

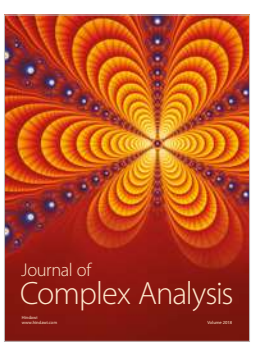

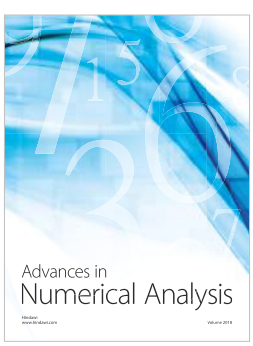

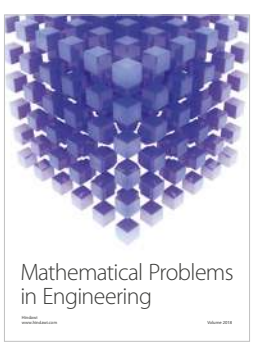

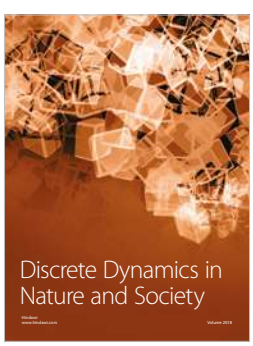

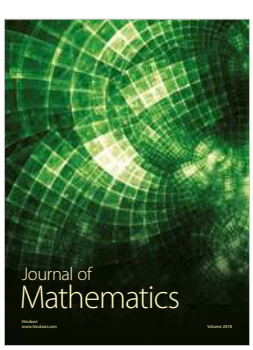

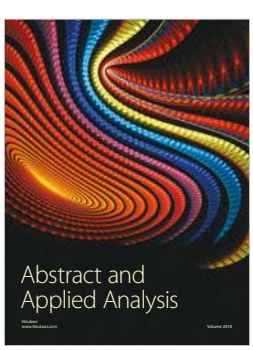

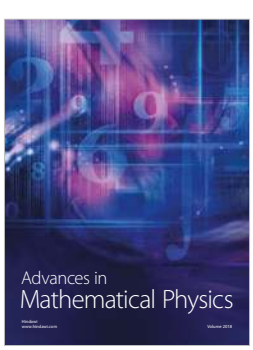

Hindawi

Submit your manuscripts at
www.hindawi.com